

# Matrix Density Engineering of Hydrogel Nanoparticles with Simulation-Guided Synthesis for Tuning Drug Release and Cellular Uptake

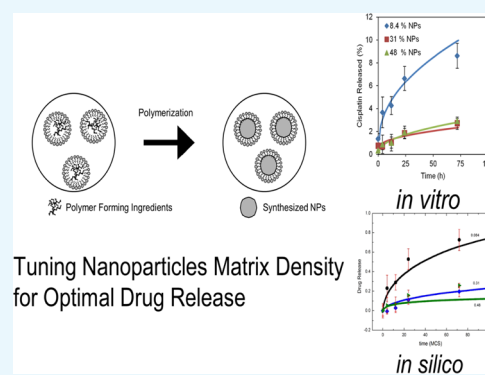
Tepei Shirakura,<sup>†,§</sup> Christof Smith,<sup>†,||</sup> Thomas John James Hopkins,<sup>†</sup> Yong-Eun Koo Lee,<sup>†,⊥</sup> Filippos Lazaridis,<sup>‡</sup> Panos Argyrakis,<sup>‡</sup> and Raoul Kopelman<sup>\*,†,⊥</sup>

<sup>†</sup>Department of Chemistry, The University of Michigan, 930 N. University Avenue, Ann Arbor, Michigan 48109, United States

<sup>‡</sup>Department of Physics, University of Thessaloniki, 54124 Thessaloniki, Greece

## Supporting Information

**ABSTRACT:** The use of a nanoparticle (NP)-based antitumor drug carrier has been an emerging strategy for selectively delivering the drugs to the tumor area and, thus, reducing the side effects that are associated with a high systemic dose of antitumor drugs. Precise control of drug loading and release is critical so as to maximize the therapeutic index of the NPs. Here, we propose a simple method of synthesizing NPs with tunable drug release while maintaining their loading ability, by varying the polymer matrix density of amine- or carboxyl-functionalized hydrogel NPs. We find that the NPs with a loose matrix released more cisplatin, with up to a 33 times faster rate. Also, carboxyl-functionalized NPs loaded more cisplatin and released it at a faster rate than amine-functionalized NPs. We performed detailed Monte Carlo computer simulations that elucidate the relation between the matrix density and drug release kinetics. We found good agreement between the simulation model and the experimental results for drug release as a function of time. Also, we compared the cellular uptake between amine-functionalized NPs and carboxyl-functionalized NPs, as a higher cellular uptake of NPs leads to improved cisplatin delivery. The amine-functionalized NPs can deliver 3.5 times more cisplatin into cells than the carboxyl-functionalized NPs. The cytotoxic efficacy of both the amine-functionalized NPs and the carboxyl-functionalized NPs showed a strong correlation with the cisplatin release profile, and the latter showed a strong correlation with the NP matrix density.



## INTRODUCTION

The tuning of pharmacokinetics and pharmacodynamics is always a challenge in the drug development and formulation process. The idea of delivering the desired concentration of drugs into targeted locations in the body over time utilizing nanoparticles (NPs) has attracted the attention of many people. This is especially true in the field of cancer therapy, vaccine, and tissue regeneration because of the tissue-targeting ability of the NPs and the tunable release of drugs inside of the NPs.<sup>1,2</sup>

Many groups have developed various types of nanoplatforms for drug delivery, such as poly(lactic-co-glycolic) acid (PLGA),<sup>3</sup> hyaluronic acid,<sup>4</sup> lipids,<sup>5–7</sup> or block copolymers.<sup>8,9</sup> Our group has made various types of polyacrylamide-based NPs (PAA-NPs) for cancer diagnosis<sup>10–14</sup> and therapy<sup>14–17</sup> because of their ideal characteristics as a platform drug delivery system. PAA-NPs have proven to be biocompatible both *in vitro* and *in vivo*.<sup>15,18</sup> In addition, the hydrophilicity and the surface charge of PAA-NPs can be easily manipulated by changing the type and relative ratio of acrylamide derivative monomers in the synthesis.<sup>19</sup> Such high engineerability also allows the conjugation of many different types of cancer-targeting moieties onto the surface of PAA-NPs for active targeting.<sup>15,20</sup> We

previously showed that hydrogel NPs loaded with cisplatin, an antitumor drug, could target SKOV3 ovarian cancer, and they successfully shrunk the tumor size, whereas free cisplatin had no effect at all on the tumor growth because of the known cisplatin resistance of the tumor.<sup>15,21</sup>

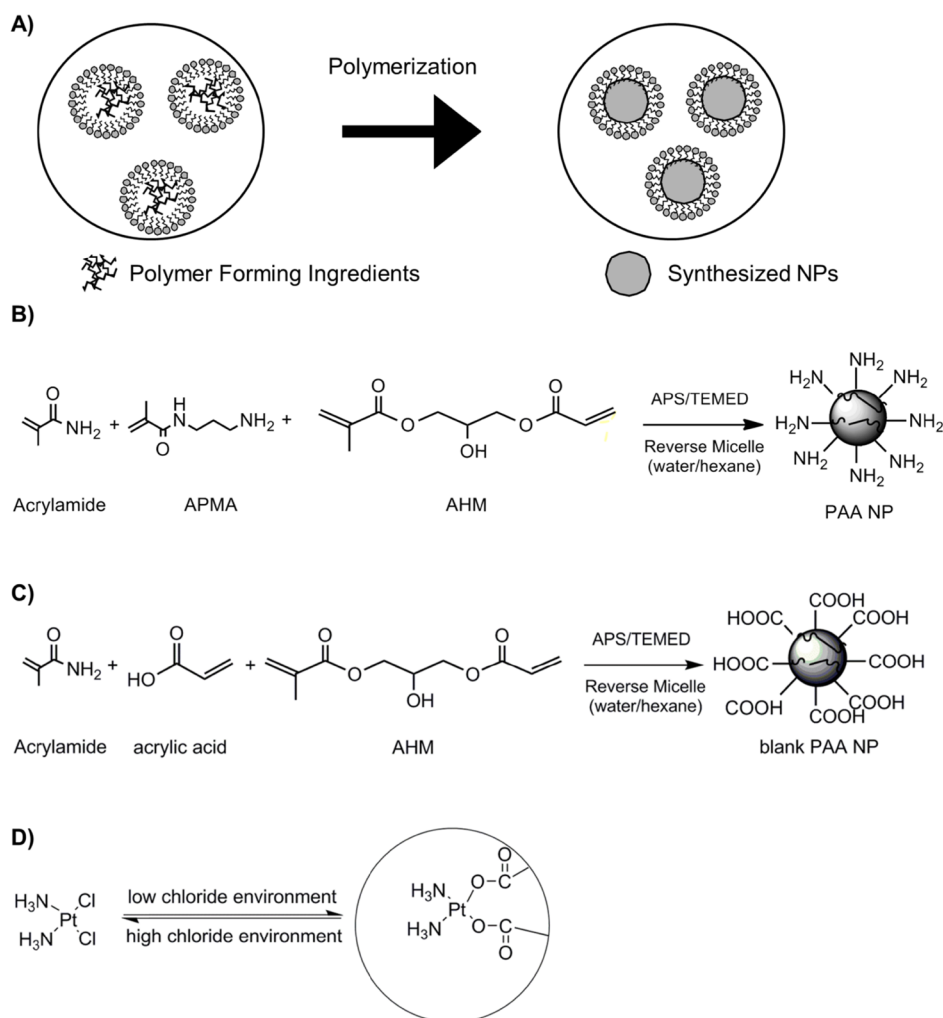
Kinetically controlled release of drugs is important for optimal drug delivery so that the NPs do not release drugs while still circulating in the blood stream and cause side effects but release most of the drugs when reaching the targeted area.<sup>5</sup> Such a temporally and spatially controlled release behavior can avoid, or at least reduce, the side effects that are associated with globally high doses of the drug.<sup>20</sup>

Temporally controlled delivery can be achieved by changing the matrix mesh size, porosity, tortuosity, and/or hydration rate.<sup>22,23</sup> In hydrogel-based drug delivery systems, the mesh size plays an important role.<sup>20,24,25</sup> The mesh size ( $\xi$ ), which is the distance between two polymeric chain cross-linkers, can be defined by eq 1<sup>24</sup>

Received: May 11, 2017

Accepted: June 30, 2017

Published: July 10, 2017

Scheme 1. Synthesis Scheme of Amine- or Carboxyl-Functionalized Hydrogel NPs<sup>a</sup>

<sup>a</sup>(A) Illustration showing the hydrogel-forming ingredients trapped inside of the water droplets surrounded by micelles in the hexane bath. After the polymerization, NPs are formed with the size of the micelle. (B) Polymerization reaction scheme for p(AAm-co-APMA)NPs. (C) Polymerization reaction scheme for p(AAm-co-AA)NPs. (D) Reaction scheme showing that cisplatin chemically and reversibly binds to the NPs via the carboxyl groups of the NPs. Abbreviations: AAm, acrylamide; AA, acrylic acid; APMA, *N*-(3-aminopropyl)methacrylamide; and AHM, 3-(acryloyloxy)-2-hydroxypropylmethacrylate

$$\xi = Q^{1/3} \left[ C_n \frac{2\overline{M}_C}{M_r} \right]^{1/2} \quad (1)$$

Here,  $Q$  is the swell ratio of the matrix,  $C_n$  is the Flory characteristic ratio of the hydrogel, which describes the flexibility of the chain,<sup>26</sup>  $\overline{M}_C$  is the average molecular weight of a chain between cross-linkers, and  $M_r$  is the molecular weight of a repeating unit. NPs with a bigger mesh size release the drugs faster.<sup>25</sup> Zhou et al. reported the control of the release profile of various small molecules using the layer-by-layer coating of polyethylenimine and acrylic acid (AA).<sup>27</sup>

The cross-linkers can be classified into two types: chemical and physical ones. In typical hydrogel NPs, they coexist.<sup>23</sup> Chemical cross-linkers, such as tetraethylene glycol dimethacrylate,<sup>24</sup> or poly(ethylene glycol)dimethacrylate,<sup>28</sup> form rigid connections between polymer chains via covalent bonding. On the other hand, physical cross-linkers form weak and reversible connections.<sup>23</sup> Some examples are hydrogen bonding, ionic bonding, and crystallite formations.<sup>23</sup>

A typical approach to change the mesh size (i.e., tune the drug release kinetics) is by varying the relative ratio of “chemical” cross-linkers to monomers in the hydrogel.<sup>24,28</sup> This approach changes the distance between the cross-linkers by varying the number of chemical cross-linkers and the mole fraction of cross-linkers.

Here, we changed the mesh size of the PAA-NPs by varying the “physical” cross-linking while maintaining the degrees of chemical cross-linking and evaluated their drug release profiles. The adjustment of the physical cross-linking was achieved by changing the polymer matrix density. Even though the effect of hydrogel density on the drug release profile has been previously studied in bulk hydrogel,<sup>23</sup> to the best of our knowledge, this concept has not been extensively studied in NPs. With the NPs prepared in the above-mentioned way, one can change the mesh size more drastically than by the method of adjusting the ratio of the chemical cross-linkers because a drastic reduction of chemical cross-linkers typically ends up in an unstable nanoparticle structure.<sup>29</sup>

Table 1. Summary of NP Formulations<sup>a</sup>

		(A) NP composition			
p(AAm-co-APMA)	mol %	p(AAm-co-AA) #1	mol %	p(AAm-co-AA) #2	mol %
AAm	81.3	AAm	81.3	AAm	71.5
APMA	2.5	AA	2.5	AA	15.2
AHM	16.2	AHM	16.2	AHM	13.3
		(B) NP polymer matrix density			
p(AAm-co-APMA) (%)		p(AAm-co-AA) #1 (%)		p(AAm-co-AA) #2 (%)	
8.4		16		4.9	
31		25		21	
48		40		34	

<sup>a</sup>(A) Composition of NPs in different categories; (B) Three different densities for each distinct composition of NPs.

A reverse micelle polymerization method was utilized for the synthesis of PAA-NPs with similar size but different matrix densities because this method controls the size of the NPs by the formed micelle size, but little by the NP ingredients, within the range of concentrations of NP ingredients we employed in this study.<sup>15,30</sup>

Utilizing this system, we evaluated the effect of changing the polymer matrix density of the NPs on drug release profile, using an antitumor drug, cisplatin, as a model drug in two commonly used forms of PAA-NPs as NP models: amine-functionalized and carboxyl-functionalized.<sup>15,19,31</sup> Amine-functionalized NPs are widely used for their high cellular uptake and ease of chemical conjugation,<sup>13–16</sup> whereas carboxyl-functionalized NPs are reported to be able to chemically and reversibly conjugate cisplatin into their matrix.<sup>31</sup> We thus chose to evaluate NPs with these two matrices. Carboxyl-functionalized NPs loaded more cisplatin and released more cisplatin, per gram of NPs, in a given time, than amine-functionalized NPs. Also, for further detailed understanding of drug release from the polymer matrix, Monte Carlo computer simulations were performed. Notably, however, the synthesized NPs showed similar cisplatin-loading capacities regardless of the polymer matrix density, but, on the other hand, the kinetics of their cisplatin release showed an inverse relationship with the polymer matrix density, for both types of NPs. In other words, we were able to successfully change the release profile of cisplatin from the NPs while maintaining their drug-loading ability. Also, we evaluated the effect of different surface functionalizations of the NPs on their cellular uptake, the cellular uptake being another important aspect of the cytotoxicity of NPs. We investigated both NP cell uptake and the cytotoxicity on a *cisplatin-resistant cell line*, SKOV3.<sup>15</sup> We found that the NP surface groups with a negative charge resulted in enhanced NP cell uptake, which enhances the cytotoxicity (as does the improved drug release), requiring one to make a balanced choice as to the optimization of cell kill efficacy.

## RESULTS AND DISCUSSION

The cisplatin-loaded NPs were prepared in two steps: (1) synthesis of blank NPs and (2) postloading of cisplatin into the blank NPs. In the postloading method, blank NPs were mixed with a high concentration of cisplatin—which would disrupt the microemulsion system for the preloading method used in our previous synthesis<sup>15</sup>—enabling a high loading of cisplatin.

**Temperature Dependence of Cisplatin Loading.** To efficiently load cisplatin into the NPs, we investigated the effect of the loading temperature on the wt % loading of cisplatin,

which is defined by eq 2. We compared the loading of cisplatin at two different temperatures, for amine-functionalized NPs, utilizing the blank p[acrylamide (AAm)-co-N-(3-aminopropyl)-methacrylamide (APMA)] NPs. High temperature is known to help in improving the loading efficiency and to prevent the potential aggregation of NPs during the loading.<sup>4</sup> When cisplatin was loaded at room temperature (22 °C), the loading of cisplatin was 0.58%, whereas when cisplatin was loaded into NPs at higher temperature (90 °C), the temperature reported by the Howell group,<sup>4</sup> the loading was 5.63%. Thus, almost 10 times higher loading of cisplatin was achieved at the elevated loading temperature. The higher the temperature, the more flexible the NP matrix becomes; thus, the cisplatin molecules can migrate further inside of the hydrogel NPs.<sup>31</sup> A similar temperature dependency of cisplatin loading was observed for carboxyl-functionalized NPs, which is consistent with the work previously reported by the Howell group using a carboxyl acid containing sugar, hyaluronic acid, as a carrier of cisplatin.<sup>4</sup> Because of this high loading, we chose 90 °C as the loading temperature for the rest of the experiments.

**Synthesis of PAA-NPs of Varying Polymer Matrix Densities.** To adjust the polymer matrix density, NPs were synthesized with the reverse micelle (water-in-oil) emulsion method (Scheme 1A). In our system, the nanosized water droplets, which contained monomers and cross-linkers (Table 1A), were coated by surfactants in the hexane bath. Free-radical polymerization was performed so as to form NPs inside of the water droplets. The size of the synthesized NPs was determined by the ratio among the water phase, hexane phase, and surfactants. In this way, we can tune the matrix density of the synthesized NPs by changing the NP ingredient concentration (Table 1B) in the water droplet while unchanging the size and molar composition of the synthesized NPs to be constant (Table 1A).

The compositions of the NPs and their estimated matrix densities are summarized in Table 1. For each of the compositions of the NPs, three different concentrations of the reaction ingredients in the water phase were employed. The NP polymer matrix density in Table 1B is estimated by the following equation

$$\rho = \frac{A}{A + B} \times 100 (\%) \quad (2)$$

Here,  $\rho$  is the polymer matrix density (A.U.),  $A$  is the weight of the hydrogel-forming ingredients, and  $B$  is the weight of aqueous solvent during the synthesis (1.3 mL of water and 1 mL of water and 0.77 mL of dimethylformamide (DMF) for

Table 2. Cisplatin Loading to the p(AAm-co-APMA) NPs with Different Polymer Matrix Densities<sup>a</sup>

	blank			cisplatin-loaded			
	size (nm)	PDI	ζ-potential (mV)	size (nm)	PDI	ζ-potential (mV)	wt % loading
8.4% NPs	40 (±0)	0.25 (±0.01)	10.3 (±1.6)	41 (±5)	0.27 (±0.02)	15.1 (±1)	4.7 (±0.5)
31% NPs	47 (±3)	0.23 (±0.06)	18.1 (±0.9)	37 (±1)	0.19 (±0.03)	18.7 (±4.1)	5.9 (±0.8)
48% NPs	63 (±1)	0.16 (±0.04)	30.5 (±1.9)	55 (±9)	0.17 (±0.07)	35.9 (±6.5)	5.2 (±0.7)

<sup>a</sup>The densities of NPs are defined by percentage, using eq 2. PDI, polydispersity index.

amine-functionalized NPs and carboxyl-functionalized NPs, respectively).

**Loading of Cisplatin to p(AAm-co-APMA) of Varying Polymer Matrix Densities.** First, p(AAm-co-APMA) NPs of three different matrix densities were synthesized (Scheme 1B) and were loaded with cisplatin. The results of the loading are summarized in Table 2. Interestingly, the wt % loading of cisplatin did not change with the variation in the matrix density. The size of the NPs shrunk after being loaded with cisplatin, possibly because cisplatin screens the electrostatic repulsion between the positive amine-functionalized chains of the matrix,<sup>23</sup> or cisplatin may act as a cross-linker that weakly connects the matrix chains by van der Waals forces.

Next, we confirmed that the shrinkage of the size was not due to the degradation of NPs. The size of blank NPs (no cisplatin) actually slightly increased, from 51 (±1) nm with PDI of 0.11 (±0.01) to 70 (±1) nm with PDI of 0.17 (±0.01), after these NPs were exposed to 90 °C for 4 h.

The sizes of the cisplatin-loaded NPs of different matrix densities were similar, as expected, because the sizes of the micelles during the synthesis were also similar. No notable change of ζ-potential was observed after the loading of cisplatin.

**Release Profile of Cisplatin-Loaded p(AAm-co-APMA) NPs.** The release profiles of cisplatin from p(AAm-co-APMA) NPs of different matrix densities were investigated (Figure 1). The cisplatin-loaded 8.4% NPs showed significantly higher percentage release of cisplatin than cisplatin-loaded 31% and cisplatin-loaded 48%, which results from the loose matrix structure. However, we did not observe a significant difference in the % release of cisplatin between 48% NPs and 31% NPs.

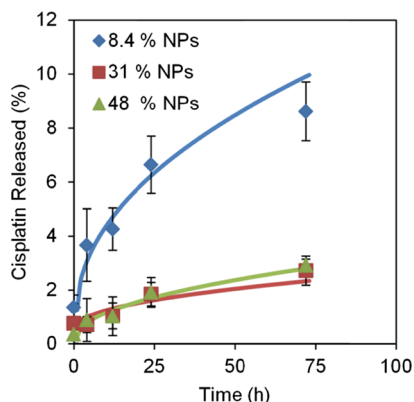


**Figure 1.** Cisplatin release from cisplatin-loaded p(AAm-co-APMA) NPs over time. The dots represent the experimental data, whereas the lines represent the fitted curve, using eq 3. Percentage representation of NPs shows different polymer matrix densities. Note that the absolute release pattern is similar to the % release pattern, within error, due to the similar loadings of the three NP classes, that is, the 8.4% NPs give the highest release, by far.

The change in the polymer matrix density from 48 to 31% may not be significant enough to observe a notable change in the release profile. We did not observe complete release in any of the formulations we tested, probably because some cisplatin molecules are buried deep inside of the matrix, where the interaction between the cisplatin molecules and the matrix is stronger than in the area closer to the surface. However, it is reported that the drugs slowly released over time even with a rigid matrix; therefore, it is expected that the cisplatin release continues over time.<sup>27</sup>

To further quantitatively evaluate the result, the Peppas equation<sup>32</sup> was applied to fit each of the release curves and thus calculate the effective diffusion coefficient ( $D$ ). The data fit is shown in Figure 1.

$$\frac{M_t}{M_\infty} = 1 - \frac{6}{\pi} \sum_{n=1}^{\infty} \frac{1}{n^2} \exp\left[-\frac{Dn^2\pi^2t}{a^2}\right] + C \quad (3)$$

Here,  $\frac{M_t}{M_\infty}$  represents the release ratio at time  $t$ ,  $D$  is the effective diffusion coefficient of cisplatin,  $a$  is the radius of the NPs, and  $C$  is the fraction of cisplatin that is released during the initial burst release.

The calculated diffusion coefficients  $D$  are summarized in Table 3. The 8.4% NPs have the highest value of  $D$ . This may

**Table 3.** Effective Diffusion Coefficient of NPs of Varying Densities

NP density (%)	$D$ ( $10^{-23} \text{ m}^2 \text{ s}^{-1}$ )	$R^2$
8.4	0.11	0.96
31	$3.3 \times 10^{-3}$	0.77
48	$1.7 \times 10^{-2}$	0.91

be attributed to the 8.4% NPs having the lowest density. The non-monotonicity of the three  $D$  values might be attributed to the small  $R^2$  value for the 31% NPs. Expectedly, as the density of the NPs goes down, the diffusion coefficient of cisplatin increases.

**Construction of p(AAm-co-AA) NPs.** As a next step, we chemically conjugate cisplatin to NPs to increase the cisplatin loading by using a carboxyl acid containing monomer, AA, as one of the ingredients of the NPs.<sup>31</sup> We prepared the p(AAm-co-AA) NPs so as to evaluate the effect of the functional group, in the acrylamide derivative monomer, on the loading and release of cisplatin (Scheme 1C). It has been reported that cisplatin chemically binds to the carboxyl groups in the absence of the  $\text{Cl}^-$  ion (Scheme 1D).<sup>33</sup> In the presence of  $\text{Cl}^-$ , such as in the body, or in the presence of  $\text{H}_3\text{O}^+$ , such as inside cellular lysosomes, the carboxyl group, initially binding to the platinum center of the cisplatin, was replaced by  $\text{Cl}^-$  or  $\text{H}_3\text{O}^+$ , which results in the release of cisplatin from the NPs.<sup>31,34</sup>

Initially, we constructed NPs by using the same composition as for the p(AAm-co-APMA) NPs, except substituting APMA

Table 4. Cisplatin Loading into p(AAm-co-AA) NPs at Different Matrix Densities<sup>a</sup>

	blank			cisplatin-loaded			wt % loading
	size (nm)	PDI	ζ-potential (mV)	size (nm)	PDI	ζ-potential (mV)	
4.9% NPs	135 (±5)	0.28 (±0.03)	-39.9 (±2.7)	98 (±2)	0.26 (±0.08)	-44.8 (±2)	11.4 (±0.2)
21% NPs	39 (±1)	0.26 (±0.03)	-35.8 (±1.9)	39 (±2)	0.39 (±0.14)	-51 (±5.3)	9.9 (±0.9)
34% NPs	36 (±1)	0.16 (±0.01)	-45.6 (±5.7)	43 (±3)	0.24 (±0.06)	-46 (±1.6)	10.3 (±2.1)

<sup>a</sup>The densities of the NPs are defined by percentage using eq 2.

with AA, without changing the molar ratio of the composing ingredients [p(AAm-co-AA) #1 of Table 1]. Into these NPs, cisplatin could not be loaded either at room temperature or at higher temperatures. These NPs formed aggregates during the loading procedure, possibly due to the loss of surface charge, presumably because of too much consumption of carboxylic groups by cisplatin. Therefore, the molar percentage of AA was increased (2.5 to 15%), whereas the amount of cross-linkers was reduced from 16 to 13% so as to increase the stability of p(AAm-co-AA) #2, as shown in Table 1. The NPs of the modified composition were also prepared at three different matrix densities, and then, we loaded cisplatin into these NPs.

When cisplatin was loaded into the above NPs at high temperature, no aggregation was observed, whereas for the loading at room temperature, aggregation of the NPs was observed. Also, it was reported<sup>34,55</sup> that cisplatin can be more easily loaded into the carboxyl group containing NPs under basic conditions. Therefore, cisplatin was loaded into NPs in the presence of 25 mM NaOH. The results of the loading are summarized in Table 4. The sizes of the NPs were measured after loading with cisplatin. The 21% NPs and 34% NPs showed relatively similar NP sizes (Table 4). On the other hand, the 4.9% NPs had considerably larger sizes than the other two NPs. This could be because of the swelling of the NPs because of the low cross-linking of their matrix, as well as their high negative charge in the aqueous solvent, where there is no surfactant to restrict their size. Because the 4.9% NPs are 4 times bigger in size than the other NPs (Table 4), the density of 4.9% is expected to be 8 times lower than the theoretical density.

To understand the relationship of the polymer matrix density and the diffusion coefficient, the cisplatin release profiles of the 21% NPs and 34% NPs, which have similar NP sizes, were evaluated (Figure 2).

As we observed in the case of the p(AAm-co-APMA) NPs, 21% NPs released more cisplatin than the 34% overall. The effective diffusion coefficients ( $D$ ) of the NPs were calculated, using eq 3, so as to understand the relationship between the polymer matrix density of the NPs and their effective diffusion coefficient. To calculate the effective diffusion coefficient, the released cisplatin at each time point was subtracted from the percentage of cisplatin released during the initial burst.

The 34% NPs had a smaller effective diffusion coefficient than the 21% NPs, which is consistent with our intended NP design and their release profile data (Figure 2). Also, confirming our expectations, carboxyl-functionalized NPs of lower polymer matrix density release cisplatin at a faster rate. These observations give some new insights into the swelling behavior of environment-responsive NPs. The polymer matrix density had an inverse correlation with the release kinetics (or mesh size), and this indicates the potency of upper critical solution-like NPs as drug carriers.<sup>31</sup> On the other hand, the 21% NPs had an initial burst release of cisplatin, possibly due to their loose matrix. We are not aware of a theory explaining this

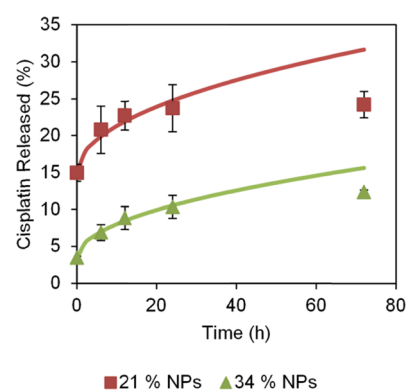


Figure 2. Cisplatin release from cisplatin-loaded p(AAm-co-AA) NPs over time. The dots represent the experimental data, whereas the lines represent the fitted curves, using eq 3. Percentage representation of NPs shows different polymer matrix densities. The experimental data, up to 24 h, were used to fit the data. The original (time 0) cisplatin concentrations are given in Table 6.

burst release.<sup>36</sup> This implies that the initial burst release is a phenomenon that is inversely correlated with the polymer matrix density. It indicates that a similar burst release might occur in environment-responsive NPs, and environment-responsive NPs might release a significant amount of drugs rapidly, immediately after the surrounding environment changes.

We then evaluated the release profile of the 4.9% NPs to understand the effect of the larger size of these NPs. The 4.9% NPs had 1.1% of initial burst release and released 10% of the cisplatin inside within 72 h. The 4.9% NPs had a higher effective diffusion coefficient, whereas the 21% NPs showed the fastest release kinetics. The latter is presumably due to the size difference between the 4.9% NPs and 21% NPs; the 4.9% NPs are 2.5 times larger than the 21% NPs, on average (Table 5). The larger size of an NP slows down the release kinetics from that NP because the cisplatin molecules need to migrate over a longer distance inside of the NP (eq 3).

Table 5. Effective Cisplatin Diffusion Coefficients for the p(AAm-co-AA) #2 NPs of Varying Densities

NP density (%)	$D$ ( $10^{-23}$ m <sup>2</sup> s <sup>-1</sup> )	$R^2$	size (nm)
4.9	0.63	0.96	98 (±2)
21	0.39	0.94	39 (±2)
34	0.25	0.99	43 (±3)

**Simulation Methods and Results.** We now perform computer simulations for the processes described in the previous sections, as an alternate approach for monitoring the rate of the drug release. Simulations of this type have been extensively performed in the past,<sup>37,38</sup> albeit for different experimental systems. We briefly describe here the model used. We consider a matrix made of a two-dimensional square lattice

of size  $L \times L$  sites, where  $L$  is the length of the square. Drug particles (cisplatin molecules) are randomly placed on the lattice sites and are allowed to diffuse with time, taking steps only to adjacent sites. If a drug molecule reaches the perimeter of the matrix, then it is permanently removed from the system. A certain number of the lattice sites are designated as obstacles, meaning that they are blocked sites that are hindering the particle motion. These obstacles give a measure of the difficulty that the moving molecules have on their way to be released by reaching the lattice perimeter. They can also be thought of as a measure of the mobility of the drug molecules. Thus, if a drug particle diffuses toward a blocked site, then it must bounce back and must subsequently find an open site to diffuse into. The drug particles are randomly placed on lattice sites with the initial drug concentration  $\rho_0$ , avoiding double occupancy. Particle diffusion is simulated by selecting particles at random and moving them randomly to one of the nearest-neighbor sites. A particle is removed from the system when it migrates through one of the perimeter sites. The obstacle sites are also randomly distributed in the system with concentration  $\rho_s$ . Time is counted in Monte Carlo steps, where one (1) such step constitutes one movement, on the average, for all particles present. We monitor the number of particles released from the system as a function of time. We average the results over 100 different realizations.

To see the effect of the obstacles during diffusion, we simulate the drug release for several different concentrations  $\rho_s$ . We show the results in Figure 3. We use an initial

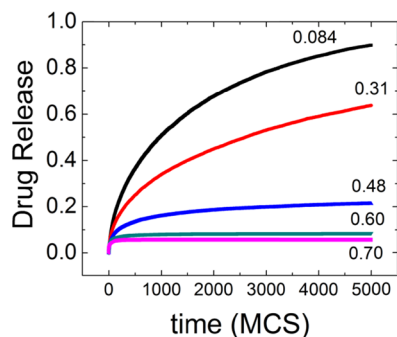


**Figure 3.** Drug Release Fraction vs time, for several values of  $\rho_s$ , which expresses the polymer matrix density. We used a square lattice with  $L = 100$ . The initial concentration of particles (equivalent to drug loading) is  $\rho_0 = 0.02$ .

concentration of drug particles,  $\rho_0 = 0.02$ , and we vary  $\rho_s$ . We observe that as  $\rho_s$  is increased the drug released is decreased, and interestingly, it reaches a plateau for values of obstacles  $\rho_s > 0.50$ .

The concentration (mole fraction) of cisplatin molecules (drug) in the simulation was chosen to be the same as the experimental data, by using Table 6. Note that these mol % data express the input fraction of the drug/(drug + monomer + cross-linker). We now use the following parameters,  $\rho_0 = 0.02$

**Table 6.** Varying NP Matrix Densities of p(AAm-co-APMA) and Their Cisplatin Loading in mol %

polymer matrix density (%)	cisplatin loading (mol %)
8.4	1.6
31	2
48	1.7

and  $\rho_s$  equal to the matrix density of the NPs, in an effort to simulate the experimental system. For the amine-functionalized NPs, we have five points of experimental data for three different matrix densities (0.084, 0.31, and 0.48). Each point is the fraction of cisplatin released after a certain amount of time (h). To have a common normalization, we divide the experimental data by 10 (this is similar to dividing the simulation results by 10 and the experimental data by 100). We then fit one point of the experiment with one point of the simulation. For example, for the experimental point (12, 0.1039), if the simulation point of 0.1039 release is achieved after 258 Monte Carlo steps, we normalize by multiplying the simulation time by 12/258. Finally, we subtract the initial burst release (release at time zero) from all experimental values to achieve zero release at zero time.

In Figure 4, we present the results for  $\rho_s = 0.084, 0.31$ , and 0.48. The NP sizes are  $41 (\pm 5)$ ,  $37 (\pm 1)$ , and  $55 (\pm 9)$  nm. To

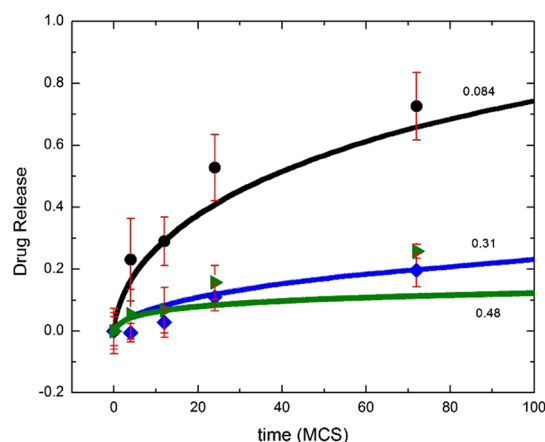


**Figure 4.** Drug Release Fraction vs time, for  $\rho_s = 0.084, 0.31$ , and 0.48. The initial concentration of particles is  $\rho_0 = 0.02$ . The points are the experimental measurements, whereas the lines are the computer simulations.

simulate the different NP sizes, we used different lattice sizes ( $L = 100, 90$ , and 134), assuming that 41 nm corresponds to  $L = 100$ . We can clearly see that the simulation is in good agreement with the experiment for the cases of matrix densities equal to 0.084 and 0.310. For the matrix density of 0.480, the agreement is good at early times, but not so good at later times. This may happen due to the fact that in our simulation, when the concentration of obstacles is too large, many particles stay totally (or almost totally) trapped and cannot escape the lattice. It is likely that a similar phenomenon occurs in the experiment but for lower values of matrix density than in the simulation.

In addition to the parameter values reported here, we used different values for the initial particle concentration  $\rho_0 = 0.20$  and 0.50. We also tried different lattice sizes  $L = 50, 100$ , and 200. Last, we tried subtracting the initial burst release from the rest of the values. For all of the above, the results show similar patterns.

**Comparing the Cellular Uptake of Amine-Functionalized NPs and Carboxyl-Functionalized NPs.** Cellular uptake is another important aspect of designing a highly effective drug delivery system because releasing drugs inside of the cells means that drugs are released closer to the site of action, as well as that the NPs may overcome the multidrug resistance of cancer cells.<sup>39,40</sup> We evaluated how the difference in the surface of NPs affects the cellular uptake. The cellular

uptake of cisplatin was compared between cisplatin-loaded 31% p(AAm-co-APMA) NPs and cisplatin-loaded 21% p(AAm-co-AA) NPs, where the percentages refer to the polymer matrix density defined by eq 2 (Figure 5).

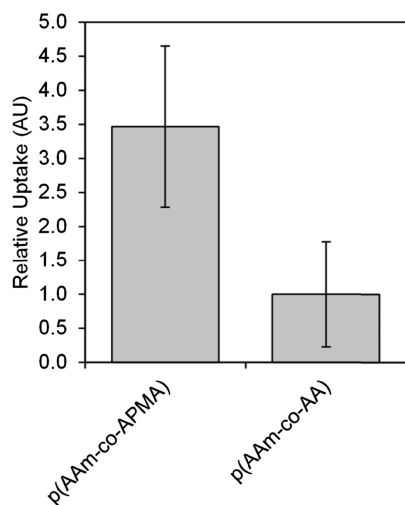


**Figure 5.** Cellular uptake study of cisplatin from positively charged NPs and negatively charged NPs. The data are normalized to the cellular uptake of p(AAm-co-AA). The 31% p(AAm-co-APMA) NPs and 21% p(AAm-co-AA) NPs were picked for the experiment; the percentages refer to the polymer matrix density.

There is an almost 3.5 times higher uptake of cisplatin when p(AAm-co-APMA) NPs were used as drug carriers than when p(AAm-co-AA) NPs were used. This higher cellular uptake of p(AAm-co-APMA) NPs is probably due to the preferable interaction of amine-functionalized NPs with cellular membranes by electrostatic interactions, as well as by the enhancement by albumin.<sup>41,42</sup> It should be noted that the possibility of agglomeration was evaluated in complete RPMI using 48% p(AAm-co-APMA) NPs as representative NPs. Even though the size has been increased from 63 nm (Table 2) to 114 ( $\pm 2$  nm) with a PDI of 0.26 ( $\pm 0.01$ ) because of the formation of a protein-NP complex, no sign of severe agglomeration was observed.<sup>42</sup>

We also calculated the absolute cisplatin uptake of SKOV3 to be 22 ( $\pm 8$  fg/cells) and 9.0 ( $\pm 7$  fg/cells) for p(AAm-co-APMA) and p(AAm-co-AA), respectively. This corresponds to less than 0.18% of the incubating cisplatin, typically of what has been previously observed to happen.<sup>43</sup>

**Cytotoxicity of Cisplatin-Loaded NPs.** Finally, the cytotoxicity of blank (Figures S1 and S3) and cisplatin-loaded (Figures S4 and S5) p(AAm-co-APMA) NPs and p(AAm-co-AA) NPs was evaluated. No significant indication of cytotoxicity was observed from the NPs in the absence of cisplatin. On the other hand, cisplatin-loaded NPs showed dose-dependent cytotoxicity, and p(AAm-co-APMA) NPs showed a clear dependency of their cytotoxicity. Also, the cytotoxicity of free cisplatin was evaluated (Figure S2). The calculated  $IC_{50}$  was 0.7  $\mu\text{g/mL}$ .

The difference in the cellular uptake (Figure 5) seems to explain the similarity of  $IC_{50}$  of p(AAm-co-AA) NPs to that of p(AAm-co-APMA) NPs (Figures S4 and S5), regardless of the significant difference in the release profiles. The 3.5 times difference in the NP cellular uptake between these two NP formulations could be the reason for their equal cytotoxic effect

even though the p(AAm-co-AA) NPs can release 5 times more cisplatin in 72 h than the p(AAm-co-APMA) NPs. The higher release per NP appears to be compensated by a higher NP uptake.

## SUMMARY AND CONCLUSIONS

Controlling the release kinetics from NPs is important for improving the efficacy of drugs and reducing the side effects. Specifically, our interest was to evaluate how tuning of the NP matrix density, which controls the mesh size of the NP matrix, controls the release profile of cisplatin from hydrogel NPs. This issue was elucidated by both experiment and simulations, which illustrate quantitatively the relation between the matrix density and the drug release rate. Both methods show an initial fast release at early times, which slows down at later times, and they are in good agreement. Experimentally, we used a simple method of changing the polymer matrix density, utilizing reverse micelle polymerization. Two different formulations, the amine-functionalized NPs [p(AAm-co-APMA) NPs] and the carboxyl-functionalized NPs [p(AAm-co-AA) NPs], were tested for their release profile and cellular uptake as a function of their polymer matrix density, as defined by eq 2. Both formulations showed high cisplatin loading, and the change in the polymer matrix density did not cause a change in the loading ability. Also, both formulations showed an inverse relationship between their polymer matrix density and their effective cisplatin diffusion coefficient, a critical factor that determines the release kinetics from NPs. The NPs with a loose matrix showed up to 33 times faster cisplatin diffusion in the matrix, that is, faster release. The p(AAm-co-AA) NPs had a higher loading of cisplatin, as well as a faster and higher release of cisplatin, than the p(AAm-co-APMA) NPs. However, the p(AAm-co-AA) NPs made with a low polymer matrix density had a higher initial burst release. In case the burst release is an undesirable characteristic for potential clinical applications, one method to prevent this problem is to prewash the NPs with a solvent close to the physiological condition so as to remove the cisplatin that contributes to the burst release.<sup>36</sup> The p(AAm-co-APMA) NPs showed 3.5 times higher cellular uptake than the p(AAm-co-AA) NPs presumably because of their amine functionalization, which can facilitate the cellular uptake via an electrostatic interaction with cell membranes, as well as because of potential assistance by albumin.<sup>41,42</sup> A precise control of the drug release, which can be achieved by controlling the NP polymer matrix density, as well as the cellular uptake, should enhance the efficacy of NP-assisted chemotherapy. Our cell toxicity study showed some correlation between the matrix densities of the NPs with the drug efficacy. No difference in drug efficacy was observed between p(AAm-co-APMA) NPs and p(AAm-co-AA) NPs, presumably because the high cell uptake of the amine-functionalized NPs, the p(AAm-co-APMA) NPs, was compensated by the higher cisplatin release of the carboxyl-functionalized NPs, the p(AAm-co-AA) NPs.

## EXPERIMENTAL PROCEDURES

**Materials.** Cisplatin was purchased from Selleck Chemicals LLC. RPMI growth medium was purchased from Invitrogen. *N*-(3-Aminopropyl)methacrylamide was purchased from Polysciences, Inc. All other chemicals were purchased from Sigma-Aldrich. The deionized (DI) water used in this experiment was

purified prior to the experiment, using a Milli-Q system from Millipore.

**Preparation of Blank Poly(AAm-co-APMA) NPs.** P-(AAm-co-APMA) NPs were synthesized using a reverse micelle polymerization technique by modifying the previously described method.<sup>15</sup> Briefly, 1.6 g of dioctyl sulfosuccinate (AOT) and 3.47 mL of Brij-30 were added to 45 mL of argon-purged hexane and continued to be stirred and argon-purged for 20 min in a round-bottom flask. AAm, APMA hydrochloride, and 3-(acryloyloxy)-2-hydroxypropylmethacrylate (AHM) were dissolved in 1.3 mL of water in the mol ratio reported in Table 1 and in the amount calculated using eq 2, and all mixtures were added to the flask and stirred and purged for additional 20 min. The polymerization was initiated by adding 100  $\mu$ L of 10(w/v)% ammonium persulfate (APS) and *N,N,N',N'*-tetramethylethylenediamine (TEMED). After 2 h, the polymerization was terminated by introducing atmospheric oxygen. Hexane was removed by rotary evaporation. The remaining products were washed five times with 150 mL of ethanol and five times with 150 mL of water in an Amicon stirred cell (Millipore) using a 300 kDa MW cutoff membrane. The obtained solution was filtered through a 0.2  $\mu$ m pore size filter and lyophilized for 72 h for long-term storage.

**Preparation of Blank Poly(AAm-co-AA) NPs.** p(AAm-co-AA) NPs were synthesized similar to that of the p(AAm-co-APMA) NPs but with slight modifications. AOT (4.8 g) and 9.5 mL of Brij-30 were added to 120 mL of argon-purged hexane and continued to be stirred and purged with argon for 40 min. A mixture of AAm, AA, and AHM, which was dissolved in 1 mL of DI water and 0.77 mL of DMF, was added to the flask in the mol ratio reported in Table 1 and in the amount calculated using eq 2, argon-purged for additional 20 min, and then, the polymerization was initiated by adding 100  $\mu$ L of 50 (w/v)% APS and TEMED. After 4 h, the polymerization was terminated by introducing atmospheric oxygen. Hexane was removed by rotary evaporation. The remaining products were washed seven times with 150 mL of ethanol and five times with 150 mL of water in an Amicon stirred cell (Millipore) using a 300 kDa MW cutoff membrane. The obtained solution was filtered through a 0.2  $\mu$ m pore size filter and lyophilized for 72 h for long-term storage.

**Loading of Cisplatin into Blank NPs.** NPs (10 mg) were mixed with 2 mg of cisplatin dissolved in 1 mL of water. For the loading of cisplatin to p(AAm-co-AA) NPs, 25 mM NaOH was also added to enhance the reaction between the carboxyl group in the NPs and cisplatin. In case of room-temperature loading, the mixture was kept for 3 days at room temperature. Then, unbound cisplatin was removed by washing the NPs seven times with 7 mL of water using a 100 kDa MW cutoff centrifugal membrane (Millipore). In case of high-temperature loading, the mixture was kept in a 90 °C oil bath for 4 h. Then, unbound cisplatin was removed, using the same procedure as for the NP preparation in the case of the room-temperature loading. The amounts of cisplatin loaded onto the NPs were quantified using inductively coupled plasma-optical emission spectroscopy (ICP-OES).

**Degradation Study of NPs at a Higher Temperature.** The NPs were suspended in phosphate-buffered saline (PBS) at a concentration of 10 mg mL<sup>-1</sup>, heated, and kept at 90 °C for 4 h. After cooling down the solution to room temperature, the NPs were diluted to 2 mg mL<sup>-1</sup>, and their sizes were measured using a Delsa Nano C analyzer (Beckman Coulter).

**Size and  $\zeta$ -Potential Measurement.** Dynamic light scattering was applied to measure the hydrodynamic size and the  $\zeta$ -potential of NPs using a Delsa Nano C analyzer. The size of the NPs was measured in PBS (pH 7.4) and in complete RPMI, whereas the  $\zeta$ -potential of the NPs was measured in water.

**Cisplatin Release Study.** The amount of cisplatin released from the NPs over 72 h was evaluated in PBS (pH 7.4). NP suspensions in PBS were prepared in the way similar to that of the concentration of cisplatin (25  $\mu$ g/mL). Six Eppendorf tubes (1.5 mL) containing cisplatin-loaded NPs in PBS were prepared. The tubes were kept at 37 °C until specific time points were reached: 0, 6, 12, 24, and 48 h. At each of the specific time points, the solution in the tube was filtered using a 100 kDa MW cutoff centrifugal membrane, and the filtrate was collected. The other tube was used to measure the total cisplatin concentration in the tube. The cisplatin concentrations in the filtrates were quantified using ICP-OES.

**Cellular Cisplatin Uptake Assay.** The human ovarian cancer cell line, SKOV3, was cultivated in RPMI with supplementation of 1% of penicillin, streptomycin, and glutamine and 10% of heat-inactivated fetal bovine serum (HI-FBS). SKOV3 cells were cultivated in a 100  $\times$  20 mm Petri dish to over 80% confluency. Cisplatin-loaded NPs (700  $\mu$ L) were prepared in PBS with a cisplatin concentration of 25  $\mu$ g/mL and mixed with cells in a Petri dish containing 5 mL of complete RPMI. The cells were incubated with NPs for 12 h and harvested after that. The populations on the Petri dishes were counted, and the cells were lysed with nitric acid. The Pt content in the lysate was measured using ICP-OES. On the basis of the cell population and Pt content in the cell lysate, the Pt content per cell was calculated.

**Statistical Analysis.** Statistical analysis was performed using Microsoft Excel (Microsoft, Redmond, WA) and GraphPad Prism 7.00 (GraphPad Software, La Jolla, CA).

## ■ ASSOCIATED CONTENT

### 📄 Supporting Information

The Supporting Information is available free of charge on the ACS Publications website at DOI: 10.1021/acsomega.7b00590.

Cytotoxicity of blank p(AAm-co-APMA) NPs, cytotoxicity of free cisplatin to SKOV3 ovarian cancer cell line, cytotoxicity of blank p(AAm-co-AA) NPs, cytotoxicity study of cisplatin-loaded p(AAm-co-APMA) NPs, and cytotoxicity study of cisplatin-loaded p(AAm-co-AA) NPs (PDF)

## ■ AUTHOR INFORMATION

### Corresponding Author

\*E-mail: [kopelman@umich.edu](mailto:kopelman@umich.edu) (R.K.).

### ORCID

Raoul Kopelman: 0000-0002-7770-8272

### Present Addresses

<sup>§</sup>Glycomine, Inc., 953 Indiana St. San Francisco, CA 94080, USA (T.S.).

<sup>||</sup>Department of Microbiology and Immunology, UNC School of Medicine, Marsico Hall, 125 Mason Farm Rd. Chapel Hill, NC 27599, USA (C.S.).

<sup>†</sup>Department of Chemistry, Hanyang University, Seoul, 04763, Republic of Korea (Y.-E.K.L.).

## Notes

The authors declare no competing financial interest.

## ACKNOWLEDGMENTS

Financial Support was provided by the Rackham Graduate School and a National Institutes of Health grant, R21NS084275 (R.K.). The authors thank James Windak of the Michigan Chemistry Instrument Shop for his instrumental support.

## REFERENCES

- (1) McMillan, J.; Batrakova, E.; Gendelman, H. E. Cell Delivery of Therapeutic Nanoparticles. In *Progress in Molecular Biology and Translational Science*, 1st ed.; Elsevier Inc., 2011; pp 563–601.
- (2) Koutsopoulos, S. Molecular fabrications of smart nanomaterials and applications in personalized medicine. *Adv. Drug Delivery Rev.* **2012**, *64*, 1459–1476.
- (3) Dhar, S.; Gu, F. X.; Langer, R.; Farokhzad, O. C.; Lippard, S. J. Targeted delivery of cisplatin to prostate cancer cells by aptamer functionalized Pt(IV) prodrug-PLGA-PEG nanoparticles. *Proc. Natl. Acad. Sci. U.S.A.* **2008**, *105*, 17356–17361.
- (4) Li, S.-D.; Howell, S. B. CD44-targeted microparticles for delivery of cisplatin to peritoneal metastases. *Mol. Pharm.* **2010**, *7*, 280–290.
- (5) de Kroon, A. I. P. M.; Staffhorst, R. W. H. M.; de Kruijff, B.; Burger, K. N. J. Cisplatin nanocapsules. *Methods Enzymol.* **2005**, *391*, 118–125.
- (6) Burger, K. N. J.; Staffhorst, R. W. H. M.; de Vijlder, H. C.; Velinova, M. J.; Bomans, P. H.; Frederik, P. M.; de Kruijff, B. Nanocapsules: lipid-coated aggregates of cisplatin with high cytotoxicity. *Nat. Med.* **2002**, *8*, 81–84.
- (7) Terwogt, J. M. M.; Groenewegen, G.; Pluim, D.; Maliepaard, M.; Tibben, M. M.; Huisman, A.; Huinink, W. W. T. B.; Schot, M.; Welbank, H.; Voest, E. E.; Beijnen, J. H.; Schellens, J. H. Phase I and pharmacokinetic study of SPI-77, a liposomal encapsulated dosage form of cisplatin. *Cancer Chemother. Pharmacol.* **2002**, *49*, 201–210.
- (8) Nishiyama, N.; Koizumi, F.; Okazaki, S.; Matsumura, Y.; Nishio, K.; Kataoka, K. Differential gene expression profile between PC-14 cells treated with free cisplatin and cisplatin-incorporated polymeric micelles. *Bioconjugate Chem.* **2003**, *14*, 449–457.
- (9) Nishiyama, N.; Yokoyama, M.; Aoyagi, T.; Okano, T.; Sakurai, Y.; Kataoka, K. Preparation and Characterization of Self-Assembled Polymer–Metal Complex Micelle from cis-Dichlorodiammineplatinum(II) and Poly(ethylene glycol)–Poly( $\alpha,\beta$ -aspartic acid) Block Copolymer in an Aqueous Medium. *Langmuir* **1999**, *15*, 377–383.
- (10) Koo, Y.; Reddy, G.; Bhojani, M.; Schneider, R.; Philbert, M.; Rehemtulla, A.; Ross, B.; Kopelman, R. Brain cancer diagnosis and therapy with nanoplateforms. *Adv. Drug Delivery Rev.* **2006**, *58*, 1556–1577.
- (11) Kopelman, R.; Koo, Y.-E. L.; Philbert, M.; Moffat, B. A.; Reddy, G. R.; McConville, P.; Hall, D. E.; Chenevert, T. L.; Bhojani, M. S.; Buck, S. M.; Rehemtulla, A.; Ross, B. D. Multifunctional nanoparticle platforms for in vivo MRI enhancement and photodynamic therapy of a rat brain cancer. *J. Magn. Magn. Mater.* **2005**, *293*, 404–410.
- (12) Lee, Y.-E. K.; Orringer, D. A.; Kopelman, R. Nanoparticles for Cancer Diagnosis and Therapy. In *Polymer-Based Nanostructures*; Broz, P., Ed.; RSC Publishing: Cambridge, U.K., 2010; pp 333–353.
- (13) Orringer, D. A.; Koo, Y.-E. L.; Chen, T.; Kim, G.; Hah, H. J.; Xu, H.; Wang, S.; Keep, R.; Philbert, M. A.; Kopelman, R.; Sagher, O. In Vitro Characterization of a Targeted, Dye-Loaded Nanodevice for Intraoperative Tumor Delineation. *Neurosurgery* **2009**, *64*, 965–972.
- (14) Qin, M.; Hah, H. J.; Kim, G.; Nie, G.; Lee, Y.-E. K.; Kopelman, R. Methylene blue covalently loaded polyacrylamide nanoparticles for enhanced tumor-targeted photodynamic therapy. *Photochem. Photobiol. Sci.* **2011**, *10*, 832–841.
- (15) Winer, I.; Wang, S.; Lee, Y.-E. K.; Fan, W.; Gong, Y.; Burgos-Ojeda, D.; Spahlinger, G.; Kopelman, R.; Buckanovich, R. J. F3-Targeted Cisplatin-Hydrogel Nanoparticles as an Effective Therapeutic That Targets Both Murine and Human Ovarian Tumor Endothelial Cells In vivo. *Cancer Res.* **2010**, *70*, 8674–8683.
- (16) Hah, H. J.; Kim, G.; Lee, Y.-E. K.; Orringer, D. A.; Sagher, O.; Philbert, M. A.; Kopelman, R. Methylene Blue-Conjugated Hydrogel Nanoparticles and Tumor-Cell Targeted Photodynamic Therapy. *Macromol. Biosci.* **2011**, *11*, 90–99.
- (17) Shirakura, T.; Ray, A.; Kopelman, R. Polyethylenimine incorporation into hydrogel nanomaterials for enhancing nanoparticle-assisted chemotherapy. *RSC Adv.* **2016**, *6*, 48016–48024.
- (18) Wenger, Y.; Schneider, R. J.; Reddy, G. R.; Kopelman, R.; Jolliet, O.; Philbert, M. A. Tissue distribution and pharmacokinetics of stable polyacrylamide nanoparticles following intravenous injection in the rat. *Toxicol. Appl. Pharmacol.* **2011**, *251*, 181–190.
- (19) Qin, M.; Lee, Y.-E. K.; Ray, A.; Kopelman, R. Overcoming Cancer Multidrug Resistance by Codelivery of Doxorubicin and Verapamil with Hydrogel Nanoparticles. *Macromol. Biosci.* **2014**, *14*, 1106–1115.
- (20) Lee, Y.-E. K.; Kopelman, R. Targeted, Multifunctional Hydrogel Nanoparticles for Imaging and Treatment of Cancer. In *Multifunctional Nanoparticles for Drug Delivery Applications—Imaging, Targeting, and Delivery*; Svenson, S., Prud'homme, R. K., Eds.; Springer US: Boston, MA, 2012; pp 225–255.
- (21) Rosenberg, B.; VanCamp, L.; Trosko, J. E.; Mansour, V. H. Platinum compounds: a new class of potent antitumor agents. *Nature* **1969**, *222*, 385–386.
- (22) Washington, C. Drug release from microdisperse systems: a critical review. *Int. J. Pharm.* **1990**, *58*, 1–12.
- (23) Peppas, N. A.; Hilt, J. Z.; Khademhosseini, A.; Langer, R. Hydrogels in Biology and Medicine: From Molecular Principles to Bionanotechnology. *Adv. Mater.* **2006**, *18*, 1345–1360.
- (24) Fisher, O. Z.; Peppas, N. A. Polybasic nanomaterials prepared by UV-initiated photopolymerization. *Macromolecules* **2009**, *42*, 3391–3398.
- (25) Lin, C.-C.; Metters, A. T. Hydrogels in controlled release formulations: Network design and mathematical modeling. *Adv. Drug Delivery Rev.* **2006**, *58*, 1379–1408.
- (26) Echeverria, C.; Peppas, N. A.; Mijangos, C. Novel strategy for the determination of UCST-like microgels network structure: effect on swelling behavior and rheology. *Soft Matter* **2012**, *8*, 337–346.
- (27) Zhou, J.; Moya, S.; Ma, L.; Gao, C.; Shen, J. Polyelectrolyte coated PLGA nanoparticles: templation and release behavior. *Macromol. Biosci.* **2009**, *9*, 326–335.
- (28) Satarkar, N. S.; Hilt, J. Z. Hydrogel nanocomposites as remote-controlled biomaterials. *Acta Biomater.* **2008**, *4*, 11–16.
- (29) Chen, Y.; Ding, D.; Mao, Z.; He, Y.; Hu, Y.; Wu, W.; Jiang, X. Synthesis of Hydroxypropylcellulose-poly(acrylic acid) Particles with Semi-Interpenetrating Polymer Network Structure. *Biomacromolecules* **2008**, *9*, 2609–2614.
- (30) Poulsen, A. K.; Arleth, L.; Almdal, K.; Scharff-Poulsen, A. M. Unusually large acrylamide induced effect on the droplet size in AOT/Brij30 water-in-oil microemulsions. *J. Colloid Interface Sci.* **2007**, *306*, 143–153.
- (31) Shirakura, T.; Kelson, T. J.; Ray, A.; Malyarenko, A. E.; Kopelman, R. Hydrogel Nanoparticles with Thermally Controlled Drug Release. *ACS Macro Lett.* **2014**, *3*, 602–606.
- (32) Ritger, P. L.; Peppas, N. A. A simple equation for description of solute release I. Fickian and non-fickian release from non-swelling devices in the form of slabs, spheres, cylinders or discs. *J. Controlled Release* **1987**, *5*, 23–36.
- (33) Howe-Grant, M. E.; Lippard, S. J. Aqueous Platinum(II) Chemistry; Binding to Biological Molecules. In *Metal Ions in Biological Systems*; Sigel, H., Sigel, A., Eds.; Dekker: New York, 1980; pp 63–125.
- (34) Peng, J.; Qi, T.; Liao, J.; Chu, B.; Yang, Q.; Li, W.; Qu, Y.; Luo, F.; Qian, Z. Controlled release of cisplatin from pH-thermal dual responsive nanogels. *Biomaterials* **2013**, *34*, 8726–8740.
- (35) Ohya, Y.; Oue, H.; Nagatomi, K.; Ouchi, T. Design of macromolecular prodrug of cisplatin using dextran with branched

galactose units as targeting moieties to hepatoma cells. *Biomacromolecules* **2001**, *2*, 927–933.

(36) Huang, X.; Brazel, C. S. On the importance and mechanisms of burst release in matrix-controlled drug delivery systems. *J. Controlled Release* **2001**, *73*, 121–136.

(37) Kosmidis, K.; Argyrakis, P.; Macheras, P. A reappraisal of drug release laws using Monte Carlo simulations: the prevalence of the Weibull function. *Pharm. Res.* **2003**, *20*, 988–995.

(38) Kosmidis, K.; Argyrakis, P.; Macheras, P. Fractal kinetics in drug release from finite fractal matrices. *J. Chem. Phys.* **2003**, *119*, 6373–6377.

(39) Brigger, I.; Dubernet, C.; Couvreur, P. Nanoparticles in cancer therapy and diagnosis. *Adv. Drug Delivery Rev.* **2012**, *64*, 24–36.

(40) Biswas, S.; Torchilin, V. P. Nanopreparations for organelle-specific delivery in cancer. *Adv. Drug Delivery Rev.* **2014**, *66*, 26–41.

(41) He, C.; Hu, Y.; Yin, L.; Tang, C.; Yin, C. Effects of particle size and surface charge on cellular uptake and biodistribution of polymeric nanoparticles. *Biomaterials* **2010**, *31*, 3657–3666.

(42) Fleischer, C. C.; Payne, C. K. Secondary Structure of Corona Proteins Determines the Cell Surface Receptors Used by Nanoparticles. *J. Phys. Chem. B* **2014**, *118*, 14017–14026.

(43) Feliu, N.; Sun, X.; Puebla, R. A. A.; Parak, W. J. Quantitative Particle–Cell Interaction: Some Basic Physicochemical Pitfalls. *Langmuir* **2017**, DOI: [10.1021/acs.langmuir.6b04629](https://doi.org/10.1021/acs.langmuir.6b04629).